

Global Biogeochemical Cycles

RESEARCH ARTICLE

10.1029/2020GB006659

Special Section:

The Arctic: An AGU Joint Special Collection

Key Points:

- Tundra environments feature some of the world's most variable soils
- The occurrence and overlap of different periglacial landforms and processes create a unique spatial structure in permafrost environments
- Local scale variability in tundra soils can exceed landscape scale variability with important implications for Arctic carbon dynamics

Supporting Information:

- Supporting Information S1

Correspondence to:

M. B. Siewert,
matthias.siewert@umu.se

Citation:

Siewert, M. B., Lantuit, H., Richter, A., & Hugelius, G. (2021). Permafrost causes unique fine-scale spatial variability across tundra soils. *Global Biogeochemical Cycles*, 35, e2020GB006659. <https://doi.org/10.1029/2020GB006659>

Received 10 MAY 2020
 Accepted 7 DEC 2020

© 2021. The Authors.

This is an open access article under the terms of the [Creative Commons Attribution-NonCommercial-NoDerivs License](#), which permits use and distribution in any medium, provided the original work is properly cited, the use is non-commercial and no modifications or adaptations are made.

Permafrost Causes Unique Fine-Scale Spatial Variability Across Tundra Soils

M. B. Siewert¹ , H. Lantuit^{2,3} , A. Richter⁴ , and G. Hugelius^{5,6} 

¹Department of Ecology and Environmental Sciences, Umeå University, Umeå, Sweden, ²Alfred Wegener Institute Helmholtz Centre for Polar and Marine Research, Potsdam, Germany, ³Institute for Geosciences, University of Potsdam, Potsdam, Germany, ⁴Centre for Microbiology and Environmental Systems Science, University of Vienna, Vienna, Austria, ⁵Department of Physical Geography, Stockholm University, Stockholm, Sweden, ⁶Bolin Centre for Climate Research, Stockholm University, Stockholm, Sweden

Abstract Spatial analysis in earth sciences is often based on the concept of spatial autocorrelation, expressed by W. Tobler as the first law of geography: “everything is related to everything else, but near things are more related than distant things.” Here, we show that subsurface soil properties in permafrost tundra terrain exhibit tremendous spatial variability. We describe the subsurface variability of soil organic carbon (SOC) and ground ice content from the centimeter to the landscape scale in three typical tundra terrain types common across the Arctic region. At the soil *pedon scale*, that is, from centimeters to 1–2 m, variability is caused by cryoturbation and affected by tussocks, hummocks and nonsorted circles. At the *terrain scale*, from meters to tens of meters, variability is caused by different generations of ice-wedges. Variability at the *landscape scale*, that is, ranging hundreds of meters, is associated with geomorphic disturbances and catenary shifts. The co-occurrence and overlap of different processes and landforms creates a spatial structure unique to permafrost environments. The coefficient of variation of SOC at the pedon scale (21%–73%) exceeds that found at terrain (17%–66%) and even landscape scale (24%–67%). Such high values for spatial variation are otherwise found at regional to continental scale. Clearly, permafrost soils do not conform to Tobler’s law, but are among the most variable soils on Earth. This needs to be accounted for in mapping and predictions of the permafrost carbon feedbacks through various ecosystem processes. We conclude that scale deserves special attention in permafrost regions.

1. Introduction

Tundra terrain and soils in permafrost affected environments have a high subsurface variability (Ping et al., 2015). Understanding this variability will help to better predict the role of these landscapes in a warming climate. This is particularly relevant for soil organic carbon (SOC) storage and ground ice content, which have become key research topics in the field (Sjöberg et al., 2020). SOC stored in the circumpolar permafrost region has been estimated to ca. 1,300 ± 200 Pg (Hugelius et al., 2014), which represents approximately half the SOC stored in soils worldwide (Köchy et al., 2015). This SOC is partly frozen and particularly vulnerable to warming temperatures, which can lead to remobilization as greenhouse gases and foster further climate warming (Chadburn et al., 2017; Hugelius et al., 2020; Schuur et al., 2015). A recent study found that abrupt thaw processes causing thermokarst, ground subsidence from melting of ground ice, may double the radiative forcing of the permafrost feedback (Turetsky et al., 2020). At the same time, rising Arctic temperatures have led to Arctic greening marked by increasing trends in vegetation biomass (Epstein et al., 2012; Myneni et al., 1997), and, in this context, it is also important to understand fine-scale spatial patterns of such vegetation changes (Myers-Smith et al., 2011).

One of the most striking features of tundra environments is the widespread occurrence of patterned ground. Patterned ground refers to a set of regular or symmetric landforms that take the shape of circles, hummocks, nets, polygons, steps, and stripes (Washburn, 1956). Vast areas in the Arctic are covered by typical terrain types associated with repeating patterns of these landforms (cf. Liljedahl et al., 2016; Michaelson et al., 2008; Zoltai & Tarnocai, 1981). The scale of periglacial landforms can range from a few centimeters in diameter for small sorted circles to ice-wedge polygons with a spacing of a few decameters (Ballantyne, 2013; Ulrich et al., 2011). Sorted and nonsorted circles, hummocks and tussocks occur in tundra environments within and beyond the permafrost regions, while ice-wedge polygons occur in permafrost environments within

and beyond tundra environments even under boreal forest (e.g., Siewert, 2018; Siewert et al., 2015). The distribution of these landforms has not yet been mapped at circumpolar scale. Only the distribution of cryoturbated soils (i.e., Turbels, soils characterized by expressions of frost heave) which are associated with such landforms, is available at such scale (Figure 1a; Tarnocai et al., 2009).

The formation of these landforms and associated frost heave processes lead to fine-scale subsurface variability in soil properties (Siewert et al., 2016; Walker et al., 2008; see Ping et al., 2015 for a comprehensive review). This is closely linked to a particular mode of pedogenesis, called cryogenesis, which plays an important role in patterned ground formation. Due to differential frost heave, soil material is mixed and organic-rich material is incorporated into deeper soil layers in a process called cryoturbation (Ping, Michaelson, Kimble, et al., 2008). Therefore, cryoturbation has been linked to large stocks of SOC in the circumpolar permafrost region (Ping, Michaelson, Jorgenson, et al., 2008; Tarnocai et al., 2009). Yet, these stocks were often sampled and quantified using isolated pedons and did not capture the local scale spatial variability in the landscape.

The traditional understanding and assumption of local scale variability and spatial processes in ecology, soil sciences, and biogeochemistry often reflect Tobler's first law of geography which assumes spatial autocorrelation and states: "everything is related to everything else, but near things are more related than distant things" (Tobler, 1970). As such, spatial autocorrelation is the base of many geostatistical digital soil mapping methods (McBratney et al., 2003). Furthermore, the variability of SOC is expected to increase with scale (Goidts et al., 2009; Zhang et al., 2011). In the Arctic, spatial variability and autocorrelation of SOC have only been analyzed at regional to continental scale for Alaska (Mishra & Riley, 2015), and at fine-scale (<4 m) in the discontinuous permafrost zone (Evgrafova et al., 2018). However, we are still missing an explicit quantitative description in tundra terrain across scales and in particular at the scale of periglacial landforms (<30 m ground resolution). This is also important because we observe scale-dependency when quantifying SOC in permafrost environments which can lead to underestimation when using low-resolution spatial data (Hugelius, 2012; Siewert, 2018). Similar scale-dependency also affects vegetation productivity and is particularly relevant in heterogeneous Arctic ecosystems (Siewert & Olofsson, 2020). Recently, high-resolution remote sensing data has become increasingly available even for remote circumpolar regions (Pope et al., 2014). This enables us to explore this spatial variability in unprecedented detail. Satellite imagery with meter to submeter (2–0.5 m) resolution allows mapping of SOC at the scale of ice-wedges while maintaining spatial coverage over several square kilometers (Siewert et al., 2015), and unmanned aerial vehicles (UAVs) can resolve tundra terrain at centimeter resolution (Assmann et al., 2018; Fraser et al., 2016; Siewert & Olofsson, 2020).

With an increased interest in environmental change in the Arctic and new, highly resolved remote sensing data available, several research gaps have become apparent. To obtain a better understanding of these landscapes, we need to study their subsurface variability. This can improve upscaling studies that aim to scale soil core, plot scale or landform based findings to the landscape scale, and will assist models that explicitly incorporate periglacial processes and landforms and their long-term impact on C cycling (Aas et al., 2018; Beer, 2016). Further, it is relevant to identify the spatial and temporal scales at which periglacial processes and landforms operate and may react to climate change pressure. Deciphering spatial variability and the relationship of SOC and ground ice with scale, can thus help to better quantify the permafrost carbon feedbacks across the Arctic.

The overall aim of this work is to describe subsurface spatial variability in tundra terrain with a focus on SOC and ground ice. We analyzed three common tundra terrain types representative of vast areas in the circumpolar permafrost region: (1) hummocky tussock upland tundra (HT-Tundra), (2) nonsorted circles on upland tundra (NSC-Tundra), and (3) ice-wedge polygon terrain (IWP-Tundra). More specifically, we examined the validity of Tobler's first law of geography (Tobler, 1970) when applied to permafrost soils. We asked whether the SOC contents at small spatial scales were more related to each other than at larger scales. Using 38 soil profiles, semivariograms of SOC point measurements and quantitative exposure description, we described spatial variability at different spatial scales; from the *pedon scale* to the *terrain scale* and to *landscape scale* catenary gradients, or centimeter (0.01 m), to decameter (10 m), and to hectometer (100 m) scale. Based on our results, we developed suggestions for how process studies, spatial sampling, mapping

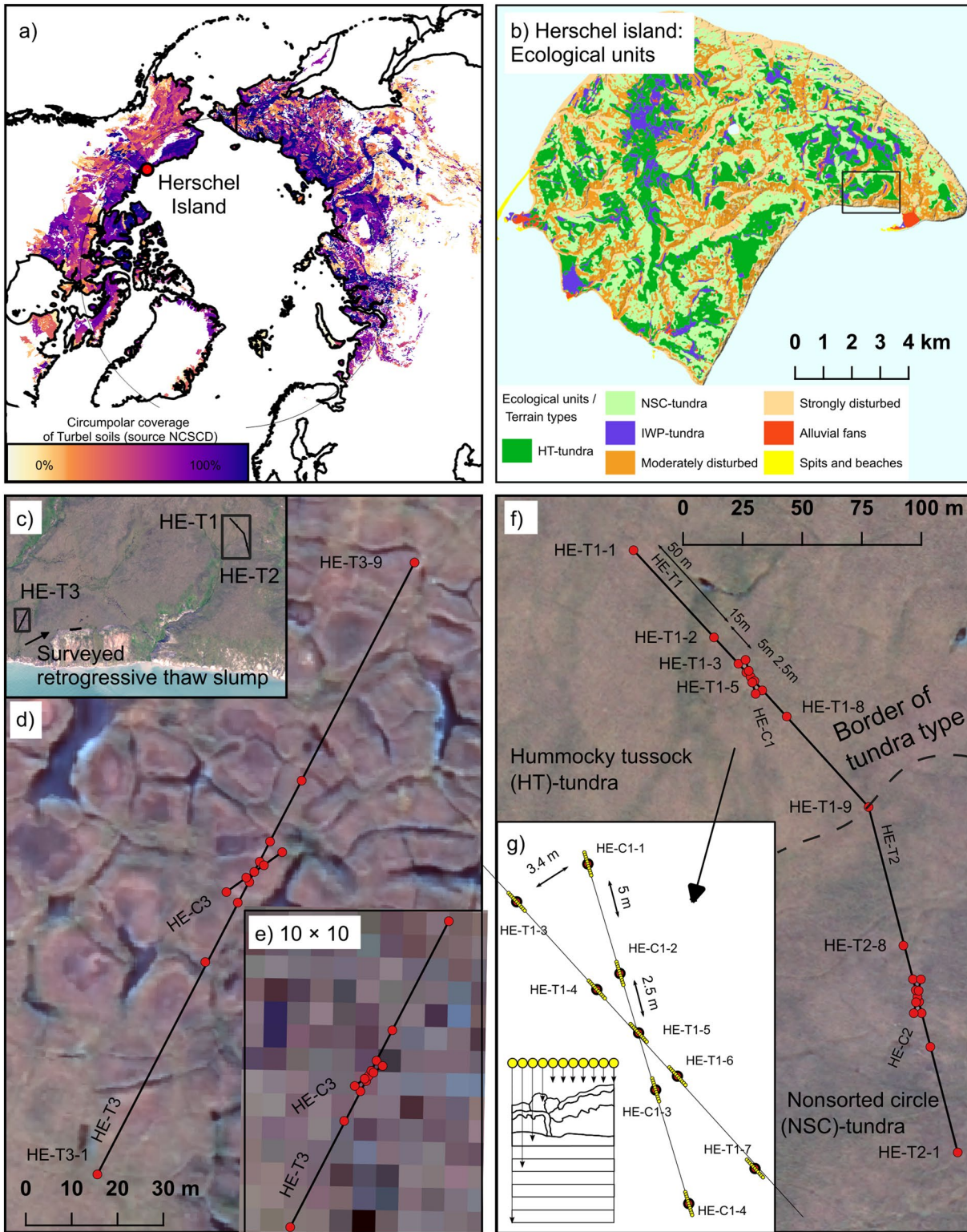


Figure 1. a) Circumpolar distribution of Turbel soils (Source: Northern Circumpolar Soil Carbon Database, Hugelius, et al., 2013; Tarnocai et al., 2009) and the location of the study area. (b) Map of Herschel Island by ecological unit (Source: Obu et al., 2015) (c) location of transects and surveyed retrogressive thaw slump, (d) ice-wedge polygon tundra (IWP-tundra) transect location showing small scale Late Holocene ice-wedges, (e) IWP-tundra at a reduced resolution of 10×10 m to reflect the improvement and potential of very high-resolution satellite imagery, (f) transect layout for hummocky tussock upland tundra (HT-tundra; top) and nonsorted circles on upland tundra (NSC-tundra; bottom). Both pictures are from a high-resolution satellite image, (g) construction of subpedons from 1 m soil pits used to calculate spatial autocorrelation. IWP, ice-wedge polygon.

and upscaling of permafrost carbon dynamics and its vulnerability can evolve to account for the unique spatial structures of permafrost and tundra environments.

2. Study Area

In this study, we used the periglacial landscape of Herschel Island (Qikiqtaruk; 69°34'N, 138°55'W, Beaufort Sea, Canada; Figures 1a and 1b) to conceptualize and describe the spatial variability of soils attributable to distinct, commonly occurring periglacial landforms. Herschel Island was particularly suited to this purpose because it was formed as a push moraine when the Laurentide Ice sheet reached its maximum northwestern extent during the Wisconsin glacialiation (Fritz et al., 2011; Mackay, 1959). Therefore, all pedological processes occurred in glacial till deposits and there has been no legacy of soil development or periglacial development prior to the last glacial maximum (LGM). Previous studies from older Beringian landscapes, showed how variability caused by Holocene processes have overprinted and interact with Pleistocene landscapes dynamics (Siewert et al., 2015, 2016; Weiss et al., 2016). However, on Herschel Island, we were able to isolate and time the analyses to post LGM dynamics. This allowed separating distinct influences on subsurface variability at separate scales.

The island covers an area of 108 km² with the highest elevation at 183 m a.s.l (Lantuit & Pollard, 2008). The mean annual air temperature is −9°C and the precipitation is 150–200 mm per year (Burn, 2012). The Holocene soils that have developed in these deformed sediments show an early Holocene thaw unconformity that has been described along the Yukon coast. This paleoactive-layer has an estimated depth of 80–90 cm on Herschel Island (Burn et al., 1986; Kokelj et al., 2002). The development of the active layer thaw depth has been studied by Burn and Zhang (2009). They found an increase in active-layer thickness of 11 cm from 2005 to 2007, resulting in 6.5 cm of ground subsidence due to the loss of ground ice. A soil and vegetation survey by Smith et al. (1989) described ecological units on Herschel Island (Figure 1b). These units took geomorphological disturbance into account and have been mapped using aerial photographs (Smith et al., 1989) and satellite imagery combined with elevation data (Obu et al., 2015). The volumetric ground ice content typically ranges between 44% to 77% (Couture & Pollard, 2017). Large scale retrogressive thaw slumps form natural exposures and allowed detailed stratigraphic investigations of the subsurface (Lantuit & Pollard, 2005, 2008; Lantuit et al., 2012). They revealed different stratigraphic units mixed by glacio-tectonic deformation. This included massive ice-bodies with sediment bands, clayic diamicton of marine origin alternating with ice-lenses, less regular clayic diamicton, and peaty silt. These had further been deformed by Holocene ice-wedges (Fritz et al., 2011, 2012).

3. Methods

3.1. Investigated Tundra Terrain Types

We designed a soil sampling scheme to analyze spatial variability of soil properties on three of the local ecological units (Figures 1c–1g). These reflect common tundra terrain types found in most circumpolar tundra environments (cf. Liljedahl et al., 2016; Michaelson et al., 2008; Siewert et al., 2015, 2016; Zoltai & Tarnocai, 1981). The tundra terrain types were characterized by their dominating periglacial landform: hummocky tussock (HT)-tundra (Figure 2a, Figure S1), nonsorted circle (NSC)-tundra (Figure 2b, Figure S2) and ice-wedge polygon (IWP)-tundra (Figures 2c, Figure S1). The soil sampling locations were chosen to represent homogeneous areas of the tundra terrain types, meaning that the transects avoided catenary transitions or spatial trends within the sampling grid.

The *HT-tundra* was characterized by very dense occurrence of cottongrass (*Eriophorum vaginatum*) tussocks forming over moss-rich earth hummocks created by cryoturbation. Locally, this terrain type is called *Herschel unit* and occurs on gentle slopes (~4%) (Smith et al., 1989). Soils had a shallow and uneven active layer mirroring surface hummocks and were either Orthic Turbic Cryosols or Gleysolic Turbic Cryosols (Canadian soil classification system; Soil Classification Working Group, 1998). These correspond to (Ruptic or Histic) Haploturbels and Aquiturbels in the U.S.D.A. Soil taxonomy system (Soil Survey Staff, 2014).

The *NSC-tundra* was dominated by nonsorted circles with discontinuous vegetation cover, alternating between exposed bare soil (15%–20%) and surrounding vegetation communities dominated by willow (*Salix sp.*) and

Dryas-Vetch in well-drained sites, and cotton grass and moss in wetter sites. This terrain type is locally called *Ko-makuk unit* and forms on smooth to undulating upland areas with a moderate slope of $\sim 7\%$ (Smith et al., 1989). Soils were moderately to imperfectly well-drained and were generally fine-textured. The dominant soil type was an Orthic Turbic Cryosol, but Regosolic Turbic Cryosols also occurred (Canadian System; Smith et al., 1989). In the Soil Taxonomy system, these are (Ruptic or Histic) Haploturbels. Large, relatively inactive mid-Holocene ice-wedges occurred under HT-tundra and NSC-tundra, but showed no or very little surface expression.

IWP-tundra can be found in areas of active or recent ice-wedge development, mainly in depressions such as drained lake basins. Ice-wedges crack in polygonal patterns forming occasionally submerged polygon centers in which sediments and peat accumulate. Depending on the degree of degradation, ice-wedge polygons, can be differentiated into low and high-centered polygons. The sampling transect was located in a drained lake basin dominated by low centered ice-wedge polygons, where ice-wedge cracking had started around 4,000 years BP (Fritz et al., 2016). The environment was wet and associated with channels of standing water over ice-wedges which resulted in contrasting vegetation communities within a short distance (mostly *Carex sp.* and *Eriophorum sp.*; Wolter et al., 2016). This terrain type is locally called *Guillemot unit* (Smith et al., 1989). The soils in polygon centers were typically Fibric Organic Cryosols with more than 40 cm of peat material over the mineral soil (Fibristels and Glacistels in the U.S.D.A. soil taxonomy). With improved drainage they transitioned into Turbic Cryosols of the Gleysolic and Orthic type (Aquiturbels and Haploturbels) (Smith et al., 1989).

3.2. Sampling Design

The sampling design aimed to reveal spatial variability at different scale levels from centimeter variability at soil horizon level, over soil pedons, tundra terrain types to landscape scale variability (hundreds of meters). We sampled 38 soil pedons following Schoeneberger et al. (2012) and an additional protocol for permafrost affected soils (Ping et al., 2013; Siewert et al., 2016). The active layer was sampled per soil horizon from 1 m wide open soil pits. A sketch of the soil horizons was drawn and later used with perspective corrected photographs to digitize the horizons (Kimble et al., 1993; Ping et al., 1997; Siewert et al., 2016). The permafrost section was sampled at the center of the soil pit by hammering a steel pipe in known depth increments into the frozen ground. We sampled to a depth of 1 m with few exceptions (e.g., when reaching an ice-wedge). Soil organic matter (SOM) content was estimated for a total of 409 bulk soil samples using the loss on ignition method burning $\sim 15\text{--}25$ ml at 550°C for 5 h (Heiri et al., 2001). The organic carbon content (OC%) was analyzed for a subset of 266 dried and ground samples using an elemental analyzer (CE Instrument EA 1110 elemental analyzer) coupled to an isotope ratio mass spectrometer (Thermo Fischer Scientific Instruments, Delta V Advantage). OC% was estimated for the remaining samples using a polynomial transfer function based on our samples for which we measured both SOM and available OC%. Values for two profiles needed to be gap-filled using soil horizon and sample depth information from neighboring profiles to reconstruct bulk density and OC%. Each sampling point was marked using a Differential Global Positioning System (DGPS). We refer to Siewert et al. (2015, 2016) for more details on soil sampling and the laboratory analyses and methods to calculate SOC storage.

The 38 soil pedons were sampled along transects in each terrain type. A main transect of 145 m length was set up with the distance of sampling points increasing from the mid-point by 2.5, 5, 15, and 50 m (Figures 1c–1g). A second shorter transect crossed at an angle of 26° at the center-point, with pedons at a distance of 2.5 and 5 m. This layout was designed to extract a large number of individual distances between sample points to investigate spatial autocorrelation, while maintaining a feasible workload given the restrictions of the remote location. The 1 m wide soil pits were aligned to the transects and subdivided in 10 cm intervals to generate 11 subpedons (Figure 1g). From the digitized soil pit sketches, the thickness of each horizon was extracted for every subpedon and used to calculate SOC stocks by matching horizons with corresponding soil samples. The SOC was then aggregated for specific depth intervals (SOC 0–100 cm, SOC

Figure 2. Top: The three typical tundra terrain types analyzed in this study. (a) Hummocky tussock (HT)-tundra (HE-C1-4), (b) Nonsorted circle (NSC)-tundra (HE-T2-2) and (c) Ice-wedge polygon (IWP)-tundra (HE-T3-05). Middle: Soil horizon distribution for typical profiles. Bottom: Corresponding soil organic carbon densities in (kg C^{-3}) per soil horizon below. The HT- and NSC-tundra showed highly disturbed soil profiles, while the IWP-tundra showed homogenous layering of organic rich peat horizons. For deep soil layers in the permafrost section only information from the core is available. For (c), the uncertainty is lower, as we can expect underlying layered lake sediments.

0–30 cm, SOC AL [active layer], SOC PF [permafrost]) and for the visible ice content. For the permafrost section homogeneous layering was applied. This allowed the creation of 418 soil subpedons for statistical analysis of the variability.

3.3. Statistical Analysis

We focused on three indicators of variability, the coefficient of variation (CV), the range and the semivariance. The CV is considered a soil spatial variability index (Weindorf & Zhu, 2010) and is defined as the ratio of the standard deviation (σ) to the mean (μ) expressed in %:

$$CV = \frac{\sigma}{\mu} \times 100$$

The range is defined as the difference between the largest ($x_{\max.}$) and smallest ($x_{\min.}$) values:

$$\text{range} = x_{\max.} - x_{\min.}$$

Range and CV were calculated for different SOC intervals, the active layer depth and the visible ice content. This was repeated at pedon scale, terrain scale and landscape scale. For CV we also calculated the 95% confidence interval (95% CI) using bootstrapping with 10,000 repetitions.

Spatial autocorrelation was examined by computing an experimental semivariogram for each terrain type using the 418 subpedon SOC values. The semivariogram displays the semivariance as a function of distance, also called lag, and is an indicator of spatial dependency (Matheron, 1963). The semivariogram $\gamma(h)$ is calculated as:

$$\gamma(h) = \frac{1}{2N} \sum_{i=1}^{N(h)} [Z(x_i) - Z(x_i + h)]^2$$

where $N(h)$ are a number of sampled data pairs of the measured variable Z at the location x_i and at a distance h from x_i . To improve the variogram, we applied log-transformation to the SOC values to normalize the data and used Cressie's modified and more robust estimator for noisy datasets (Bivand et al., 2013; Hyp-pänen, 1996). A typical semivariogram shows an initial increase in semivariance followed by stabilization indicating the distances at which no more spatial autocorrelation occurs (Sarma, 2009). It is recommended to use at least 50 or more samples for variogram analysis (Webster & Oliver, 1992). All statistical analysis were performed in R (R Core Team, 2020).

3.4. Geomorphological Transects

To show subsurface variability at meter to decameter (10 m) scale, we mapped the relative distribution of cryostratigraphic units (i.e., active layer, ice-wedges, and remaining permanently frozen sediment) from a transect section in the IWP-tundra and from retrogressive thaw slumps evolving in typical HT and NSC-tundra terrain. These retrogressive thaw slumps formed natural exposures as they erode backward along more or less semicircular to straight lines with little influence of the parent material (see also Lantuit et al., 2012). This provided an unbiased crosscut of the subsurface variability of exposed soil, sediment and ice. We surveyed the headwall by taking photographs in parallel to it. These were combined to a perspective corrected panorama picture from which the relative surface area was digitized and quantified for the active layer, ice-wedges and remaining permanently frozen sediment and ground ice. For IWP-tundra, the surface of the schematic profile was smoothed from DGPS-points and soil profiles were inserted showing the SOC density with depth for individual samples (using AQP; Beaudette et al., 2013).

4. Results

4.1. Pedon Scale Variability: Soil Horizons, Profiles, and Cryoturbation

The surface and subsurface properties of typical examples of the three tundra types are shown in Figure 2. These highlight the variability at pedon scale.

The surface HT-tundra was characterized by tussocks overgrowing repetitively occurring earth hummocks. These hummocks had an approximate radius of 40–60 cm (Figure 2a). Cryoturbation led to the occurrence of spatially variable and well-differentiated soil horizons causing SOC variability at centimeter to decimeter scale. This created significant SOC variability in the active layer, depending on the relative location of tussocks over hummocks, the distribution of surface O-horizons and active layer depth. The typical HT-tundra profile showed organic-rich horizons (*O_{ijj}/O_{ejj}/O_{ajj}*) being cryoturbated toward the landform rim, while dense mineral horizons (*B_g/B_{wg}*) were located to the center.

The surface of NSC-tundra was marked by strong expression of nonsorted circles with diameters of ~80–120 cm, often exposing bare soil at the center surrounded by grasses and shrubs grown at the edge (Figure 2b). The soil profile of this terrain type showed strongly disturbed soil horizons and significant variability of SOC. The NSC-tundra showed similar horizon types as the HT-tundra profile, but mineral horizons were more common than in HT-tundra. The subsurface variability of the SOC exceeded the visible surface variability.

For both the HT- and the NSC-tundra, the SOC density (kg C^{-3}) was unevenly distributed in the active layer section (Figure 2 bottom). Organic rich (*O**)-horizons had C% values (~20%–45%) and low dry bulk density values (~0.05–0.5 g m^{-3}), while mineral horizon had low C% (~3%–5%) values, but higher bulk densities (~1.0–1.5 g m^{-3}). In the permafrost section, C% values varied around 2%–10%, with lower background values (*C_gf* horizons) at times interrupted by cryoturbated horizons with higher C%. Bulk densities ranged at ~0.5–1.5 g m^{-3} . SOC densities declined with depth. The visible ice content varied from 10% to 100% in HT-tundra, while it averaged around 20% in NSC-tundra. In few profiles ice-wedges were cored at a depth of ~70–85 cm.

The IWP-tundra was covered by graminoids and smooth in polygon centers, but was strongly warped by ice-wedges toward the rim. The typical profile showed very homogeneous pure peat deposits (*O**-horizons) within a low centered polygon (Figure 2c). The IWP-tundra showed homogeneously accumulated peat with higher SOC densities at the top decreasing with depth. The dry bulk densities of this unit ranged from ~0.15–0.3 g cm^{-3} and C% values were ~30%–40% at the top of profiles and transitioned to ~10%–20% toward the bottom. Overall, the variability of SOC was organized at a scale that corresponded to the diameter of the ice-wedge polygon and repeated thereafter along the polygonal pattern. The active layer was shallower in this terrain type and the visible ice content was higher presumably due to the insulating effect of peat. Visible ice content averaged per profile around 20%–40% and an ice-wedge was cored once at 40 cm depth.

4.2. Terrain Scale to Landscape Scale Variability: Ice-Wedge Polygons and Exposures

The HT-tundra and NTC-tundra were underlain by a network of older, mid-Holocene, ice-wedges without significant surface expression (Figures 1f, 3a, and 3b). The variability of soil properties caused by these ice-wedges and different cryostratigraphic units is shown from a thaw slump headwall (Figure 3b). On a ~55 m stretch, with an average headwall height of ~7.5 m, the area occupied by the active layer was 9.3%. Ice-wedges occupied 17.5% of the headwall surface area and permanently frozen sediment and deformed glacial ice the remaining 73.3%. Compared to the thawed lake basin, these ice-wedges were much larger and were formed under different conditions from the mid-Holocene onward (6,500 BP) (Fritz et al., 2012). They extended into the sediments below and created a spatial disruption and deformation of the soil to depths of >7.5 m.

The variability of SOC caused by late-Holocene ice-wedges in the IWP-tundra terrain is visualized in (Figure 3c). The schematic cross-profile shows the center of an ice-wedge polygon and includes soil pedon C density data from the IWP-tundra transect. In the center, the SOC variability was almost homogeneous and dominated by the continuous accumulation of organic peat in layers. At the rim conditions were drier. The substrate still consisted of pure peat, but was replaced by ice-wedge ice at depth. Polygon troughs featured shallow soil profiles or were submerged by water (Figures 1d and 3c). The scale of the subsurface variability was dictated by the diameter of the polygons with smaller polygons creating more disruption and higher variability. Diameters varied between 5 to 20 m (Figure 1d). Ice-wedge cracking started in the late-Holocene around 4000 BP (Fritz et al., 2016).

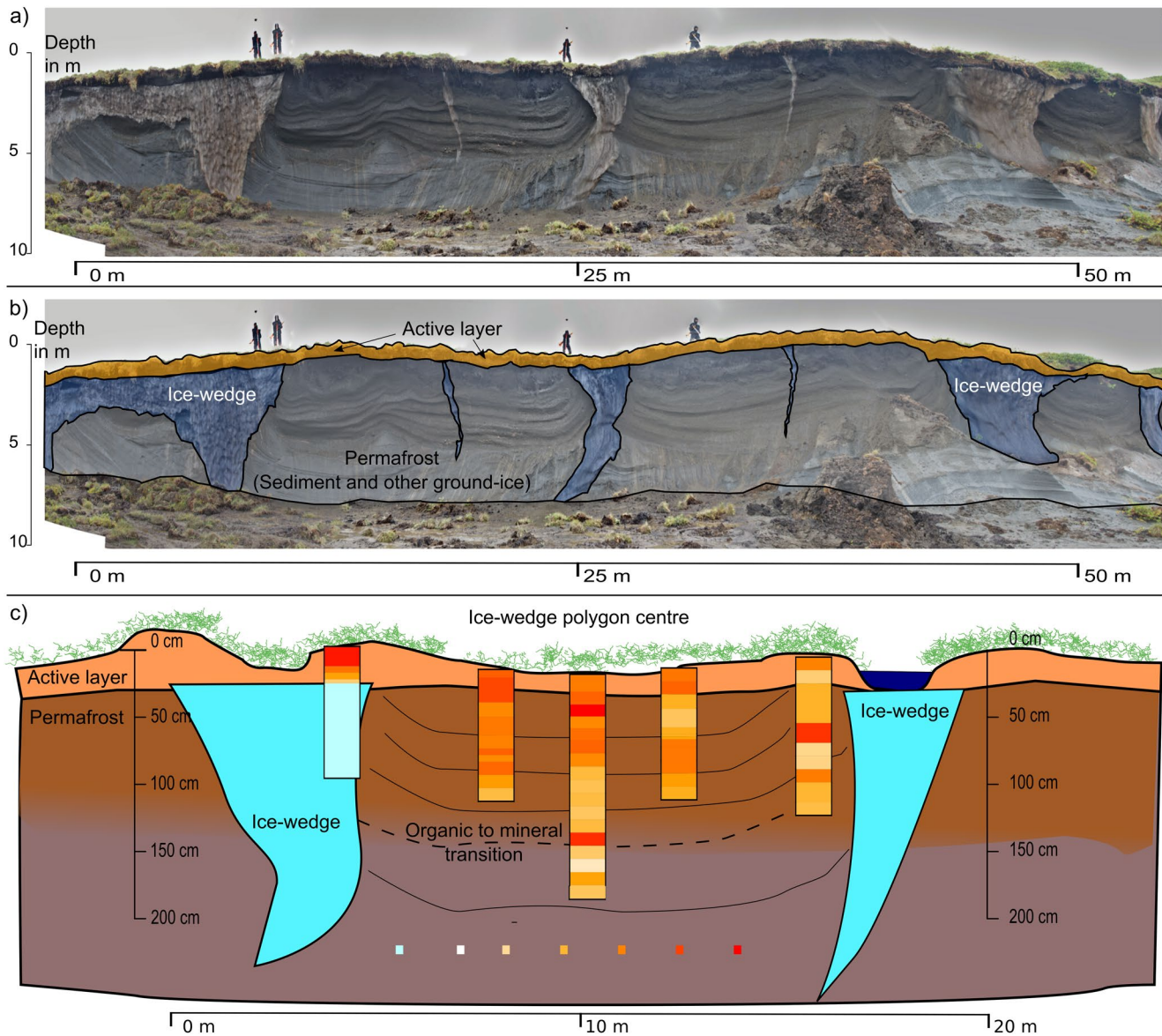


Figure 3. a) The headwall of a retrogressive thaw slump cutting into upland tundra terrain representative of HT- and NSC-tundra (person for scale). (b) Digitized overlay of the active layer (orange), ice-wedges (blue) and the remaining permafrost (white). The ice-wedge to the left was likely a crosscut through a connection point of several ice-wedges. The ice-wedge in the center had a width of 3 m, the large ice-wedge to right had a width of 7 m. The smaller ice-wedge in between had a width of 0.5 m. (c) Schematic profile across the center of the IWP-tundra transect (cf. Figure 2c top). Soil profiles show the SOC density with depth for individual samples. The organic material to mineral transition was reached for the central profile at a depth of 130 cm. Note the difference in scale for the x- and y-axis. IWP, ice-wedge polygon; SOC, soil organic carbon.

The landscape scale variability can further be documented by the diversity in ecological units or land cover classes (Figure 1b). While large land cover patches occurred, there is an overall strong fragmentation of the land cover. Topographic position and drainage caused by thermal erosion dictate terrain types in this ice-rich environment (Obu et al., 2015; Ramage et al., 2019; Smith et al., 1989).

4.3. Variability Across Scales

4.3.1. Coefficient of Variation and Range of SOC and Ice Content

We compared the variability by investigating the CV and range at three scales for these key permafrost ecosystem properties: SOC, active layer depth and visible ice content (Figure 4). The CV reached for individual

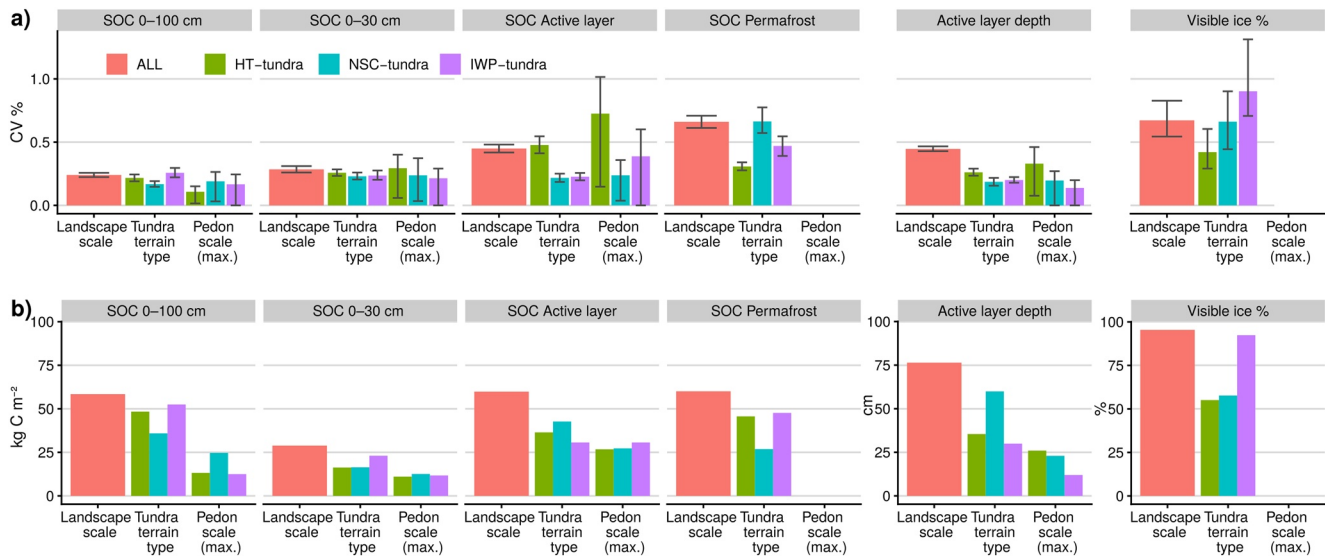


Figure 4. Variability of ecosystem variables across scales aggregated at landscape scale (all subpedons), at terrain scale (all subpedons of the respective terrain type) and the maximum found at pedon scale (all subpedons of a pedon, then max. value per terrain type). (a) Variability expressed as coefficient of variation. Error bars indicate the 95% confidence interval. (b) Variability expressed as the range between the minimum and maximum values. There is insufficient data to assess pedon scale variability in permafrost properties (only one permafrost core per pedon was collected).

variables between 24% and 67% at landscape scale for all subpedons combined. It reached similar levels for the SOC 0–100 cm and SOC 0–30 cm when subpedons were aggregated at tundra terrain type and similar maxima when subpedons were aggregated within individual soil pedons and the maximum was extracted per terrain type. For the SOC AL and SOC PF and the visible ice content, the CV was more variable among terrain types, while it was lower at terrain and pedon scale than at landscape scale for the active layer depth. The CV was highest within the permafrost section. Importantly, the CV found within individual pedons could exceed the CV found at terrain or landscape scale. The 95% CI indicate stable CV values at landscape and tundra scale, but also a wide range at pedon scale, where CV can vary substantially due to the occurrence of ground-ice replacing significant volumes of soil within single soil pedons.

The range decreased for each observed scale, but almost reached landscape scale level for the SOC 0–100, SOC PF and visible ice content within individual terrain types. The SOC AL had a larger range than the SOC 0–30 cm. NSC-tundra showed the highest active layer depth range, while IWP-tundra had the highest ice content range.

4.3.2. SOC Stocks and Ice Content

The SOC stocks and ice content variability aggregated at different scales are presented in Table 1. All values were aggregated from subpedons, thus have the same total storage. However, the standard deviation was reduced when first aggregated at pedon scale and then summarized per terrain type. When we differentiated the SOC and active layer depth by subpedon position within landforms, the SOC storage was higher in the landform rim for HT- and IWP-tundra, but lower for NSC-tundra. When aggregated at terrain scale, the HT-tundra had the highest SOC 0–100 cm storage ($49.2 \pm 10.7 \text{ kg C m}^{-2}$), followed by the IWP-tundra ($47.6 \pm 12.2 \text{ kg C m}^{-2}$). Both terrain types were not significantly different (Kruskal-Wallis sum test; $p = 0.909$). The geomorphologically disturbed NSC-tundra stored the least SOC ($39.7 \pm 6.7 \text{ kg C m}^{-2}$) in the top meter. The IWP-tundra had the largest variability of SOC values with a standard deviation of 12.2 kg C m^{-2} for the SOC 0–100 cm. It also had the pedon with the lowest SOC 0–100 cm value over an ice-wedge. The pedon with the highest SOC 0–100 cm storage (72.7 kg C m^{-2}) was located in the HT-tundra, showing the efficiency of nonsorted circles to cryoturbate SOC rich surface organic layers. The NSC-tundra had on average the deepest and most variable active layer ($71.1 \pm 13.2 \text{ cm}$), while the HT-tundra had the shallowest ($31.0 \pm 8.1 \text{ cm}$). All three terrain types had similar mean visible ice contents within the top 1 m, but showed

Table 1

Summary of the Soil Pedons, SOC Content for Several Depth Increments, Active Layer Thickness, and Average Visible Ice Content for the Three Analyzed Tundra Terrain Types

Scale	Terrain type	Pedons (^P) / Subpedons (^{SP}) (n) ^a	SOC 0–100 cm (mean ± SD)	Range SOC 0–100 cm (min.–max.)	SOC 0–30 cm	SOC active layer	SOC permafrost	Active layer thickness (cm)	Visible ice %	Visible ice % (min.–max.)
Pedon scale	HT-tundra	143 ^{SP} (13 ^P × 11)	49.2 ± 10.6	13.2	13.6 ± 2.6	13.2 ± 3.6.0	36.0 ± 10.3	31.0 ± 5.6	36.2 ± 36.2	15.3–70.3
Pedon scale	NSC-tundra	132 ^{SP} (12 ^P × 11)	39.7 ± 5.7	24.7	15.2 ± 2.6	32.6 ± 6.0	7.1 ± 4.7	71.1 ± 13.6	31.6 ± 31.6	4.7–62.3
Pedon scale	IWP-tundra	143 ^{SP} (13 ^P × 11)	47.6 ± 12.6	12.5	19.2 ± 4.4	21.7 ± 4.0	25.9 ± 12.4	35.5 ± 7.1	35.0 ± 35.0	7.7–100.0
Landform center	HT-tundra	66 ^{SP}	48.3 ± 10.2	46.9 (24.3–71.2)	12.9 ± 3.6	14.8 ± 5.9	33.5 ± 11.1	34.2 ± 7.4	36.7 ± 36.7	15.3–70.3
Landform rim	HT-tundra	77 ^{SP}	49.9 ± 11.0	48.3 (24.4–72.7)	14.2 ± 3.4	11.8 ± 6.3	38.1 ± 10.7	28.3 ± 7.8	35.7 ± 35.7	15.3–70.3
Landform center	NSC-tundra	88 ^{SP}	40.6 ± 6.2	34.6 (28.7–63.4)	15.1 ± 3.4	33.6 ± 6.6	7 ± 4.4	71.1 ± 13.4	30.6 ± 30.6	4.7–62.3
Landform rim	NSC-tundra	44 ^{SP}	37.9 ± 7.3	28.1 (27.5–55.6)	15.2 ± 3.7	30.5 ± 7.6	7.4 ± 5.5	71.2 ± 13.1	33.5 ± 33.5	4.7–62.3
Landform center	IWP-tundra	77 ^{SP}	51.8 ± 10.4	33.5 (33.2–66.7)	19.0 ± 2.2	24.2 ± 3.6	27.7 ± 10.8	38.8 ± 4.1	27.7 ± 27.7	8.3–67.8
Landform rim	IWP-tundra	66 ^{SP}	42.6 ± 12.5	43.2 (14.3–57.4)	19.5 ± 6.3	18.8 ± 4.7	23.8 ± 13.3	31.7 ± 8.0	43.5 ± 43.5	7.7–100
Tundra terrain scale	HT-tundra	143 ^{SP}	49.2 ± 10.7	48.4 (24.3–72.7)	13.6 ± 3.5	13.2 ± 6.3	36 ± 11.1	31.0 ± 8.1	36.2 ± 36.2	15.3–70.3
Tundra terrain scale	NSC-tundra	132 ^{SP}	39.7 ± 6.7	35.9 (27.5–63.4)	15.2 ± 3.5	32.6 ± 7.1	7.1 ± 4.7	71.1 ± 13.2	31.6 ± 31.6	4.7–62.3
Tundra terrain scale	IWP-tundra	143 ^{SP}	47.6 ± 12.2	52.5 (14.3–66.7)	19.2 ± 4.5	21.7 ± 4.9	25.9 ± 12.2	35.5 ± 7.1	35.0 ± 35.0	7.7–100.0
Landscape scale	ALL	418^{SP}(38^P)	45.6 ± 11.0	58.4 (14.3–72.7)	16.0 ± 4.6	22.2 ± 22.2	23.4 ± 23.4	45.2 ± 20.2	34.3 ± 34.3	4.7–100

^aFirst value indicates aggregation level. Parentheses indicate complete pedons that contributed to the subset.

Note. ^Pstands for pedon; ^{SP} stands for subpedon

Abbreviation: soil organic carbon.

considerable variability in minimum and maximum values. Ice contents did not significantly correlate with active layer thickness (Spearman's rank correlation: $p = 0.241$).

4.3.3. Spatial Autocorrelation

The empirical variograms aimed at revealing subsurface spatial autocorrelation (Figure 5). They show very high variability over short and long distances. At close range, the semivariance of SOC was slightly increasing up to 1 m, most likely reflecting soil pedon scale variability caused by soil horizons. At distances $\sim >1$ m, the variability started to increase and became periodic. These peaks were likely caused by differences in SOC storage due to patterned ground landforms and ice-wedges. For HT- and NSC-tundra, the variability remained high between peaks due to cryoturbation. In IWP-tundra, space between peaks was even, indicating spatial autocorrelation within peaty polygon centers with diameters of 2–5 m. The semivariance increased over long distances in all plots. For the combined plot for HT and NSC-tundra, the transition between tundra types at a distance >100 m becomes apparent. It is noteworthy that the semivariance repeatedly returned

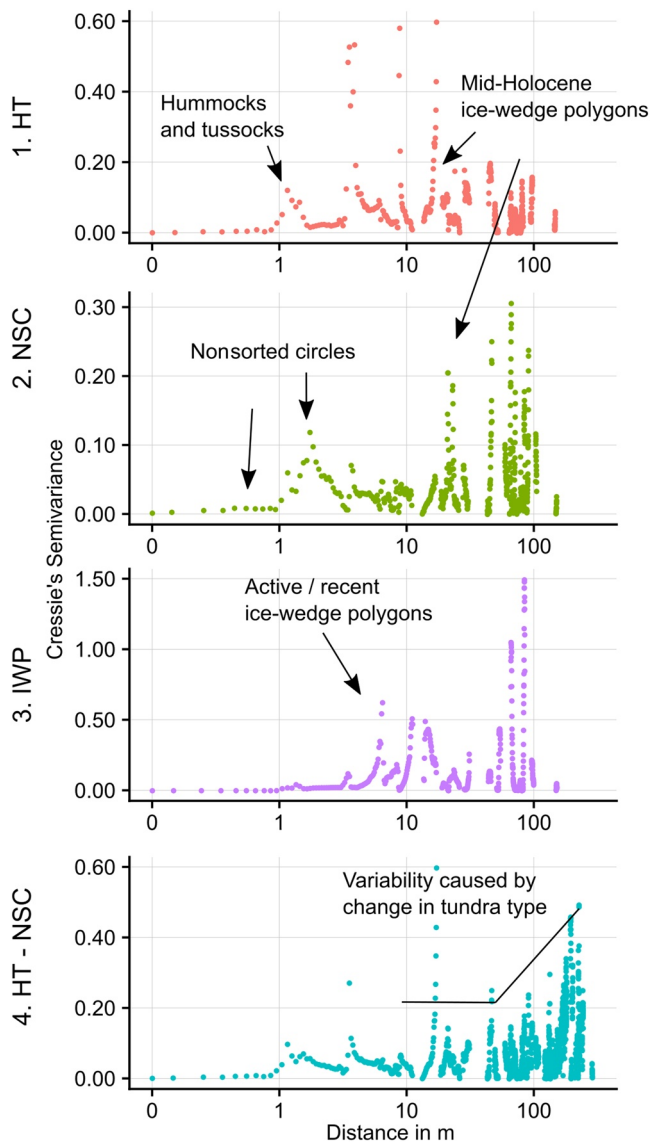


Figure 5. Semivariograms for the three different tundra types. Top to bottom: HT-tundra, NSC-tundra, IWP-tundra, HT-NSC-tundra combined (See Figure S4. For the same graph using width factor of 10 m and linear x-axis). IWP, ice-wedge polygon.

near to zero. This indicates that some pedons further apart showed more similar SOC values compared to locations near to each other. Different settings for the semivariogram parameters were tested, notably the parameter bandwidth (gstat:width), which influenced the number of points shown along the x-axis (See Figure S4.). However, all parameter settings revealed similar, uneven plots for SOC and would have led to the same overall conclusions. Modeling of a semivariogram curve failed.

5. Discussion

5.1. Variability of SOC at Different Scales

The centimeter to decimeter variability of SOC densities at the soil pedon scale was mainly caused by cryoturbation in terrain with patterned ground typical of upland tundra landscapes (i.e., earth hummocks and nonsorted circles; Figures 2 and 5). HT-tundra showed a more regular expression of this variability than the NSC-tundra (Figures 2a and 2b). In the IWP-tundra, centimeter to decimeter variability was absent in the center of ice-wedges, but was strong close to the ice-wedge rims. The permafrost exposures showed strong, binary variability (i.e., ice/no ice) of the subsoil at terrain scale (Figures 1 and 3). There were two distinct formations of ice-wedges: smaller late-Holocene ice-wedges with a spacing of approximately ~5–15 m formed in a drained lake basin and larger mid-Holocene ice-wedges in upland tundra (spacing of approximately ~15–30 m, Figure 3). The ice-wedges of the thaw lake basin were well expressed at the surface, but there was little surface expression of the older and thicker ice-wedges that were located in upland tundra terrain (Figures 1d and 1f). The terrain types also showed distinct mean SOC storage values (Table 1). Landscape scale variability was caused by transitions between tundra terrain types governed by topography, catenary gradients and differences in geomorphic disturbance regimes such as valley formation (Figures 1b and 5; Obu et al., 2015; Ramage et al., 2019).

Different periglacial processes and landforms and in particular their co-occurrence created a unique spatial structure compared to other natural environments. This formed a nested or hierarchical structure caused by an overlap of processes, both in time and space, affecting the soil properties at any given discrete point. Figure 6 provides a conceptual framework for the spatial extent of the landforms and the processes and their approximate time scales. Other relevant periglacial landforms that were shown to affect SOC variability in other Arctic environments are peat plateaus and palsas (Hugelius et al., 2011; Siewert, 2018) and major geomorphological units such as thermokarst lake basins that determine SOC storage in Yedoma terrain at hecto- to kilometer scale (Fuchs et al., 2018; Siewert et al., 2015, 2016).

5.2. Representativeness Across the Arctic

The assemblage of periglacial processes and landforms that cause subsurface variability are common across the Arctic and permafrost regions. There is abundant literature evidence of the occurrence of patterned ground landforms related to frost heave and thermal contraction cracking across the Arctic, subArctic and even boreal and alpine environments, with landforms and terrain types analogous to the described HT-, NSC- and IWP-tundra (Ballantyne, 2018; French, 2017; Warburton, 2013). This is not surprising, as these landforms are a product of thermal processes related to ground freezing ubiquitous in these regions. However, the processes also depend on other factors than temperature dynamics, such as topographic po-

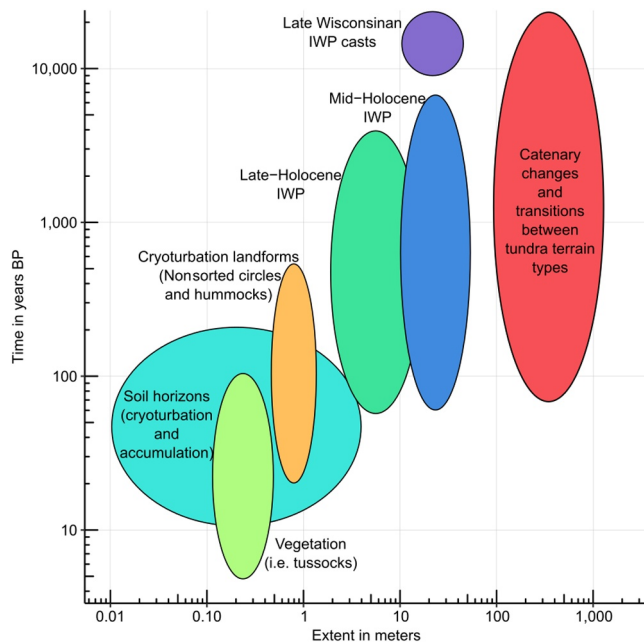


Figure 6. Conceptual diagram of spatial and temporal extent of processes and landforms causing subsurface variability in the study area. Many of these processes occur across the Arctic region. The time scale reflects an assumed minimum formation age and approximate stability under Holocene climate conditions. Reaction timing for catenary changes and terrain type variability reflects the high ground ice content facilitating potential thermokarst.

sition, soil moisture and parent material. With sufficient soil moisture available, such landforms may form in most loose soil parent material (Ballantyne, 2018; French, 2017; Warburton, 2013). Most tundra environments will likely feature at least one of these landforms and processes affecting subsurface spatial heterogeneity, and often two or more landform types will co-occur and potentially interact. Clear surface expressions of periglacial landforms are more common in tundra than in boreal forest. Many forest-tundra or boreal regions will likely feature some of this variability, but less expressed than on Herschel Island. For instance, Zoltai and Tarnocai (1981) map the occurrence of patterned ground in boreal forest (surveyed areas North of 60° in the Canadian Arctic) that seems analogous to nonsorted circles observed on Herschel Island. Maps of the Siberian region show the occurrence of frost heave and cracking for significant parts of the continuous permafrost region, including the boreal forest (Fedorov et al., 2018; Tumel and Zotova, 2019). The extent of IWP-tundra is more limited, but it is reasonable to assume that it occurs in most Arctic lowland environments of the continuous permafrost zone with high-ground ice contents (e.g., Liljedahl et al., 2016). We suggest that the current best proxy relatable to high soil variability and indirect evidence for the distribution of these landforms assemblages at circum-polar scale is likely the coverage of cryoturbated soils (i.e., Turbels) in soil maps (Figure 1a; Tarnocai et al., 2009). This may include the occurrence of hummocks, nonsorted circles that mostly occur on upland soils, while ice-wedges often dominate lowland soils. Soil conditions may differ and patterns in SOC bulk density and ice content may be site specific, but the strong variability in these soils and the lack of autocorrelation as described here is likely a common feature in moisture rich soils of the permafrost region.

5.3. A Unique Spatial Structure in Periglacial Terrain

In our study of permafrost tundra, we found variability in terms of CV of ~25%–70% even at very fine scales. For SOC 0–100 cm and SOC 0–30 cm, CV values were around 25 % while CV reached 45%–60% for the SOC AL, PF active layer depth and ground ice content. The variability was greatest in the permafrost section due to high ice content or absence thereof marked by a large range of values (4.7%–100%). In contrast, a metaanalysis of 41 studies in ecosystems worldwide comparing CV of topsoil (0–20 cm) SOC concentrations found generally low CV values < 35% and a log-linear relationship of CV with sampling area. CV values ranged from ~20 for local scale studies (<1 ha) to ~70 at regional to continental scale (Zhang et al., 2011). We found that such variability was not only achieved at the landscape scale, but also within typical tundra terrain types and within individual 1 m wide soil pedons (Figure 4 and Table 1). This indicates that tundra terrain exhibits some of Earth's most variable soils.

The semivariograms showed no spatial auto-correlation for centimeter to decameter scale, they further showed strong periodicity, caused by the strong repetitive patterns from consecutive periglacial landforms (Figure 5 and Figure S4). This periodicity is typical of spatially repeating processes, such as the repeated occurrence of an ice-wedge in a cross section, and requires appropriate geostatistical handling (Meerschman et al., 2013; Webster & Oliver, 2007). Therefore, we conclude that Tobler's first law of geography does not apply to the three analyzed tundra terrain types, as they showed no spatial decay function, but large variability expressed by CV and range values. This is in contrast to the understanding of many ecosystems worldwide (see for example Bjorholm et al., 2008; Goodchild, 2001). In particular in the upland tundra, small movement was enough to encounter the entire range of variability. This is characteristic of space without spatial dependency (Goodchild, 2001). These landscapes clearly differ from other landscapes where catenary shifts are not overprinted by patterned ground and ground properties are not disrupted by ice-wedges. Previous investigations in Alaska found a range of spatial auto-correlation of ~1,000 km when working at

a spatial resolution of 50 m (Mishra & Riley, 2015). Very local scale SOC variability within 4×4 m plots was analyzed in a forested, discontinuous permafrost area by Evgrafova et al. (2018). They found larger spatial variability for permafrost affected plots compared to nonpermafrost affected plots and a decrease in spatial heterogeneity or homogenization of SOC with a deeper active layer and very short ranges of spatial autocorrelation, mostly defined by vegetation distribution. Pedon databases also showed great variability of SOC within certain land cover classes and with depth, and high diversity of soil types (pedodiversity; Ibañez et al., 1995) within small geographic regions (Hugelius, 2012; Siewert et al., 2016). This supports our results and underlines the role of permafrost to promote freeze and thaw dynamics, leading to high SOC storage and variability at scales from centi- to decameters. Further, this questions the notion of a low pedodiversity in Arctic regions as indicated by Minasny et al. (2010).

5.4. The Relevance of Soil Variability and Permafrost Landforms for Carbon Dynamics and Ecosystem Processes in Tundra

The high variability of soil properties and the nested nature of the landform assemblage has important implications for our understanding of permafrost carbon feedbacks and Arctic greening. The distribution of SOC and ground ice are a first-order control of permafrost carbon feedbacks (Turetsky et al., 2020), and periglacial landforms and soils are important factors for the spatial organization of plant communities (Walker et al., 2008) and for aboveground ecological processes through interactions with plant roots (Iversen et al., 2015). Permafrost thaw dynamics dominate the distribution of surface water across vast land areas through the formation of thermokarst lakes, periglacial landforms and ground ice distribution (Grosse et al., 2013). Further, we have to assume that different geomorphological processes and landforms operate at different scales, independent of each other (Phillips, 1988) or interact in complex ways. Therefore, the different environmental controls of these landforms and relevant time scales need to be quantified to reduce uncertainty in projecting land surface parameters.

A wide set of environmental controls over these processes and landforms may be affected by climate change. Vegetation, such as graminoid tussocks, may respond to warming temperatures or herbivory on short and long time scales (Olofsson & Post, 2018), while nonsorted, sorted circles activity and SOC allocation by cryoturbation may be influenced by temperature amplitudes, precipitation, lithology or vegetation stabilization (D'Amico et al., 2015; Klaus et al., 2013; Palmtag & Kuhry, 2018; Walker et al., 2004). Ice-wedge formation has been linked to winter temperature variations (Matsuoka et al., 2018), but increased degradation is observed in response to climate warming even in continuous permafrost (Liljedahl et al., 2016). Landscape development and future SOC and ground ice distribution can only be quantified if the sensitivity of each these processes to a changing climate is understood. The binary response of freezing and melting/thawing points is particularly relevant. For instance, the degradation of ice-wedges can increase the micro-topographic relief with differential ground-subsidence of several decimeters (Liljedahl et al., 2016). Such micro-topography differences affect microbial communities, metabolic pathways and associated greenhouse gas fluxes (Taş et al., 2018), and has led to shrub expansion along polygonal patterns (Wolter et al., 2016). Small scale surface variability caused by cryoturbation landforms, such as nonsorted circles, was also reflected in carbon flux rates (Becher et al., 2015). This is even relevant at landscape scale, as reduced tundra vegetation productivity was linked to meter to decameter heterogeneity caused by landforms (Lara et al., 2018). Thus, the initial subsurface variability of SOC and ground ice can influence longterm greenhouse gas release in the Arctic (Faucherre et al., 2018). Several efforts have been undertaken to delineate ice-wedges and to estimate the ground ice-content (Lousada et al., 2018; Ulrich et al., 2014) and modeling efforts start to implement ice-wedges and palsas as individual entities (Aas et al., 2018; Cresto Aleina et al., 2013), but for improved understanding of Arctic greenhouse gas emissions, mapping of the circumpolar distribution of different landforms and full model integration is necessary.

5.5. Upscaling Soil Properties and Model Integration

The large variability has implications for the mapping of SOC storage and other soil properties in permafrost environments. Maps of SOC provide an important baseline to calculate SOC storage and fluxes of greenhouse gases. Present maps of SOC in the circumpolar permafrost region often use land cover and soil

maps for upscaling (e.g., Hugelius et al., 2014; Tarnocai et al., 2009). We conclude that maps generalizing and averaging over large scales, misrepresent local scale SOC variability significantly and are marked by greater uncertainty than assumed before. To make more progress, higher resolution maps predicting SOC content at the pixel level using digital soil mapping methods are necessary (Mishra et al., 2013). These methods can loosely be differentiated in three major groups: (1) geostatistical and other spatial interpolation methods mostly based on spatial autocorrelation and the distance relationship between individual points (Oliver & Webster, 2015), (2) mapping based on environmental correlations developing prediction via regression, such as many modern pixel-based machine-learning methods (Hastie et al., 2009), and (3) methods that combine both approaches (Hengl, 2009; Li & Heap, 2014; Li et al., 2011; McBratney et al., 2003).

We found that at the local scale the spatial variability of SOC content can exceed even landscape variability and no spatial autocorrelation can be detected. Therefore, upscaling methods based on spatial autocorrelation have limited ability to provide high confidence results at centimeter to decameter scale. Instead, mapping should focus on environmental correlations between soil properties and environmental variables. Multivariate ordination and other statistics indicate solid relationships in this respect (Hugelius, 2012; Hugelius & Kuhry, 2009; Hugelius et al., 2010; Siewert et al., 2015, 2016). Several variables are well correlated with SOC content and have been used for predictive mapping of SOC at different scales in permafrost environments, for example, land cover, NDVI, elevation, topographic wetness index, and various climate data (Mishra & Riley, 2015; Pastick et al., 2014; Siewert, 2018). Digital soil mapping using machine learning methods has shown good results in permafrost environments and provides the necessary alternative to spatial autocorrelation based methods (Ding et al., 2016; Siewert, 2018). A particular advantage of many machine learning methods is the possibility to handle nonlinear relationships (McBratney et al., 2003), making them perfectly suited to predict SOC in the described nested and hierarchical setting (Figure 6). Siewert (2018) compared four commonly used methods to predict SOC and found that *random forests* algorithm (Breiman, 2001) provided the best prediction model, confirming a general robustness to provide superior results in many environments (e.g., Forkuor et al., 2017; Li et al., 2011).

Furthermore, while subsurface variability can be significant, soil horizons and landforms can be used as an entity to upscale fluxes, microbial or substrate related processes. This can be done using a close-up approach as presented in Figures 2 and 3. Due to the observed variability, large replication is necessary to provide a full picture of the soil variability (Hugelius, 2012). Combined with soil properties such as SOC, N and soil texture, scaling findings from soil cores or pedons to landscape scale is possible and may also address interactions between soil horizons (e.g., Gentsch et al., 2015). In this respect, it should be easier to predict IWP-tundra properties when stratigraphically intact layers of peat can be assumed compared to HT- and NSC-tundra heavily affected by cryoturbation. Finally, there is a limited understanding of scale-linkages, that is, how large-scale processes affect small scale processes and *vice versa*. This work aims to provide a path toward such research.

6. Conclusions

We present evidence that permafrost causes a unique local scale spatial variability in Arctic soils. Clearly, for *pedon scale* to *terrain scale* analyses, Tobler's first law of geography does not apply to permafrost landscapes, as they do not feature a spatial decay function, that is spatial autocorrelation, as is the implicit understanding of many ecosystem and geographic analysis. We conclude that in tundra, small movement can be enough to encounter the entire range of SOC and ground ice content typical for that terrain type. This is due to the co-occurrence and nesting of several periglacial landforms and processes. Such conditions make permafrost environments unique compared to other regions and ecosystems where gradual landscape transitions (such as catenary shifts) are not overprinted by patterned ground. In fact, we find that tundra terrain features soils with higher variability than most other environments on Earth.

The described variability indicates that scaling of environmental properties needs to be treated carefully in these environments. Our study highlights the limitation of investigations of SOC and related dynamics that are based on single soil pedons, as well as the application of concepts and methods that are based on spatial autocorrelation. Instead, we suggest to use soil horizons and landforms as natural upscaling entities for fine-scale studies. For local-scale mapping, we suggest to focus on methods leveraging environmental

correlations such as machine-learning based methods. There is also a need to account for the nested landform assemblage and to decipher potential interactions between landforms which could result in complex trajectories for carbon dynamics. This applies to investigations in diverse fields including biogeochemical, biological, and hydrological studies. The here described variability of SOC and ground ice distribution caused by periglacial landforms underlines the urgent need to include periglacial landforms and processes in circum-Arctic investigations including earth system models.

Data Availability Statement

The soil pedon data are available from the www.pangaea.de data repository under: <https://doi.pangaea.de/10.1594/PANGAEA.927861> (<https://doi.pangaea.de/10.1594/PANGAEA.927861>).

Acknowledgments

This research was supported by the EU FP7 PAGE21 project (282700), the Swedish Research Council (VR), the EU JPI-Climate COUP project and the EU H2020 research and innovation project Nunataryuk (No 773421). We would like to thank all participants of the Yukon Coast Expedition 2015 for a successful field season and Robin Wojcik for help with processing of the soil samples. We thank the Inuvialuit people for being able to conduct research on their traditional lands. We thank the Aurora Research Institute, the Yukon Territorial Government and Yukon Parks (Herschel Island Qikiqtaruk Territorial Park) for a good cooperation.

References

- Aas, K. S., Martin, L., Nitzbon, J., Langer, M., Boike, J., Lee, H., et al. (2018). Thaw processes in ice-rich permafrost landscapes represented with laterally coupled tiles in a Land Surface Model. *Cryosphere Discuss*, *13*, 591–609. <https://doi.org/10.5194/tc-2018-210>
- Assmann, J. J., Kerby, J. T., Cunliffe, A. M., & Myers-Smith, I. H. (2018). Vegetation monitoring using multispectral sensors—Best practices and lessons learned from high latitudes. *Journal of Unmanned Vehicle Systems*, *7*, 54–75. <https://doi.org/10.1139/juvs-2018-0018>
- Ballantyne, C. K. (2013). Permafrost and periglacial features | Patterned Ground A2—Elias, Scott A. In C. J. Mock (Ed.), *Encyclopedia of quaternary science* (2nd ed., pp. 452–463). Amsterdam: Elsevier.
- Ballantyne, C. K. (2018). *Periglacial geomorphology*. John Wiley & Sons.
- Beaudette, D. E., Roudier, P., & O'Geen, A. T. (2013). Algorithms for quantitative pedology: A toolkit for soil scientists. *Computers & Geosciences*, *52*, 258–268. <https://doi.org/10.1016/j.cageo.2012.10.020>
- Becher, M., Olofsson, J., & Klaminder, J. (2015). Cryogenic disturbance and its impact on carbon fluxes in a subarctic heathland. *Environmental Research Letters*, *10*, 114006. <https://doi.org/10.1088/1748-9326/10/11/114006>
- Beer, C. (2016). Permafrost sub-grid heterogeneity of soil properties key for 3-D soil processes and future climate projections. *Frontiers of Earth Science*, *4*. <https://doi.org/10.3389/feart.2016.00081>
- Bivand, R. S., Pebesma, E., & Gómez-Rubio, V. (2013). *Applied spatial data analysis with R*. New York, NY: Springer New York.
- Bjorholm, S., Svenning, J.-C., Skov, F., & Balslev, H. (2008). To what extent does Tobler's 1st law of geography apply to macroecology? A case study using American palms (Arecaceae). *BMC Ecology*, *8*, 11. <https://doi.org/10.1186/1472-6785-8-11>
- Breiman, L. (2001). Random forests. *Machine Learning*, *45*, 5–32.
- Burn, C. R. (2012). Climate. In *Herschel island qikiqtaryuk: A natural and cultural history of Yukon's Arctic island* (pp. 48–53). Whitehorse: University of Calgary Press.
- Burn, C. R., Michel, F. A., & Smith, M. W. (1986). Stratigraphic, isotopic, and mineralogical evidence for an early Holocene thaw unconformity at Mayo, Yukon Territory. *Canadian Journal of Earth Sciences*, *23*, 794–803. <https://doi.org/10.1139/e86-081>
- Burn, C. R., & Zhang, Y. (2009). Permafrost and climate change at Herschel Island (Qikiqtaruk), Yukon Territory, Canada. *Journal of Geophysical Research*, *114*. <https://doi.org/10.1029/2008JF001087>
- Chadburn, S. E., Burke, E. J., Cox, P. M., Friedlingstein, P., Hugelius, G., & Westermann, S. (2017). An observation-based constraint on permafrost loss as a function of global warming. *Nature Climate Change*. <https://doi.org/10.1038/nclimate3262>
- Couture, N. J., & Pollard, W. H. (2017). A model for quantifying ground-ice volume, Yukon Coast, Western Arctic Canada. *Permafrost and Periglacial Processes*, *28*, 534–542. <https://doi.org/10.1002/ppp.1952>
- Cresto Aleina, F., Brovkin, V., Muster, S., Boike, J., Kutzbach, L., Sachs, T., & Zuyev, S. (2013). A stochastic model for the polygonal tundra based on Poisson–Voronoi diagrams. *Earth System Dynamics*, *4*, 187–198. <https://doi.org/10.5194/esd-4-187-2013>
- D'Amico, M., Gorra, R., & Freppaz, M. (2015). Small-scale variability of soil properties and soil–vegetation relationships in patterned ground on different lithologies (NW Italian Alps). *CATENA*, *135*, 47–58. <https://doi.org/10.1016/j.catena.2015.07.005>
- Ding, J., Li, F., Yang, G., Chen, L., Zhang, B., Liu, L., et al. (2016). The permafrost carbon inventory on the Tibetan Plateau: a new evaluation using deep sediment cores. *Global Change Biology*, *22*, 2688–2701. <https://doi.org/10.1111/gcb.13257>
- Epstein, H. E., Reynolds, M. K., Walker, D. A., Bhatt, U. S., Tucker, C. J., & Pinzon, J. E. (2012). Dynamics of aboveground phytomass of the circumpolar Arctic tundra during the past three decades. *Environmental Research Letters*, *7*, 015506. <https://doi.org/10.1088/1748-9326/7/1/015506>
- Evgrafova, A., de la Haye, T. R., Haase, I., Shibistova, O., Guggenberger, G., Tananaev, N., et al. (2018). Small-scale spatial patterns of soil organic carbon and nitrogen stocks in permafrost-affected soils of northern Siberia. *Geoderma*, *329*, 91–107. <https://doi.org/10.1016/j.geoderma.2018.05.014>
- Faucherre, S., Jørgensen, C. J., Blok, D., Weiss, N., Siewert, M. B., Bang-Andreasen, T., et al. (2018). Short and long-term controls on active layer and permafrost carbon turnover across the Arctic. *Journal of Geophysical Research: Biogeosciences*, *123*, 372–390. <https://doi.org/10.1002/2017JG004069>
- Fedorov, A. N., Vasilyev, N. F., Torgovkin, Y. I., Shestakova, A. A., Varlamov, S. P., Zheleznyak, M. N., et al. (2018). Permafrost-landscape map of the Republic of Sakha (Yakutia) on a scale 1:1,500,000. *Geosciences*, *8*, 465. <https://doi.org/10.3390/geosciences8120465>
- Forkuor, G., Hounkpatin, O. K. L., Welp, G., & Thiel, M. (2017). High resolution mapping of soil properties using remote sensing variables in South-Western Burkina Faso: A comparison of machine learning and multiple linear regression models. *PLoS One*, *12*. <https://doi.org/10.1371/journal.pone.0170478>
- Fraser, R. H., Olthof, I., Lantz, T. C., & Schmitt, C. (2016). UAV photogrammetry for mapping vegetation in the low-Arctic. *Arctic Science*, *2*, 79–102. <https://doi.org/10.1139/as-2016-0008>
- French, H. M. (2017). *The periglacial environment* (4th ed.). Chichester: John Wiley & Sons.
- Fritz, M., Wetterich, S., Meyer, H., Schirrmeyer, L., Lantuit, H., & Pollard, W. H. (2011). Origin and characteristics of massive ground ice on Herschel Island (western Canadian Arctic) as revealed by stable water isotope and Hydrochemical signatures. *Permafrost and Periglacial Processes*, *22*, 26–38. <https://doi.org/10.1002/ppp.714>

- Fritz, M., Wetterich, S., Schirmer, L., Meyer, H., Lantuit, H., Preusser, F., & Pollard, W. H. (2012). Eastern Beringia and beyond: Late Wisconsinan and Holocene landscape dynamics along the Yukon Coastal Plain, Canada. *Palaeogeography, Palaeoclimatology, Palaeoecology*, 319–320, 28–45. <https://doi.org/10.1016/j.palaeo.2011.12.015>
- Fritz, M., Wolter, J., Rudaya, N., Palagushkina, O., Nazarova, L., Obu, J., et al. (2016). Holocene ice-wedge polygon development in northern Yukon permafrost peatlands (Canada). *Quaternary Science Reviews*, 19. <https://doi.org/10.1016/j.quascirev.2016.02.008>
- Fuchs, M., Grosse, G., Strauss, J., Günther, F., Grigoriev, M., Maximov, G. M., & Hugelius, G. (2018). Carbon and nitrogen pools in thermokarst-affected permafrost landscapes in Arctic Siberia. *Biogeosciences*, 15, 953–971. <https://doi.org/10.5194/bg-15-953-2018>
- Gentsch, N., Mikutta, R., Alves, R. J. E., Barta, J., Čapek, P., Gittel, A., et al. (2015). Storage and transformation of organic matter fractions in cryoturbated permafrost soils across the Siberian Arctic. *Biogeosciences*, 12, 4525–4542. <https://doi.org/10.5194/bg-12-4525-2015>
- Goidts, E., Van Wesemael, B., & Crucifix, M. (2009). Magnitude and sources of uncertainties in soil organic carbon (SOC) stock assessments at various scales. *European Journal of Soil Science*, 60, 723–739.
- Goodchild, M. F. (2001). A geographer looks at spatial information theory. In D. R. Montello (Ed.), *Spatial information theory, lecture notes in computer science* (pp. 1–13). Springer Berlin Heidelberg. https://doi.org/10.1007/3-540-45424-1_1
- Grosse, G., Jones, B., & Arp, C. (2013). Thermokarst lakes, drainage, and drained basins. In J. F. Shroder (Editor-in-chief), R. Giardino, & J. Harbor (Eds.), *Treatise on Geomorphology, Glacial and Periglacial Geomorphology* (Vol. 8, pp. 325–353). San Diego: Academic Press.
- Hastie, T., Tibshirani, R., & Friedman, J. (2009). *The elements of statistical learning, Springer Series in statistics*. New York, NY: Springer.
- Heiri, O., Lotter, A. F., & Lemcke, G. (2001). Loss on ignition as a method for estimating organic and carbonate content in sediments: reproducibility and comparability of results. *Journal of Paleolimnology*, 25, 101–110. <https://doi.org/10.1023/A:1008119611481>
- Hengl, T. (2009). *A practical guide to geostatistical mapping of environmental variables* (2nd ed.). Luxembourg: Publications Office.
- Hugelius, G. (2012). Spatial upscaling using thematic maps: An analysis of uncertainties in permafrost soil carbon estimates. *Global Biogeochemical Cycles*, 26, GB2026. <https://doi.org/10.1029/2011GB004154>
- Hugelius, G., & Kuhry, P. (2009). Landscape partitioning and environmental gradient analyses of soil organic carbon in a permafrost environment. *Global Biogeochemical Cycles*, 23, GB3006. <https://doi.org/10.1029/2008GB003419>
- Hugelius, G., Kuhry, P., Tarnocai, C., & Virtanen, T. (2010). Soil organic carbon pools in a periglacial landscape: a case study from the central Canadian Arctic. *Permafrost and Periglacial Processes*, 21, 16–29. <https://doi.org/10.1002/ppp.677>
- Hugelius, G., Loisel, J., Chadburn, S., Jackson, R. B., Jones, M., MacDonald, G., et al. (2020). Large stocks of peatland carbon and nitrogen are vulnerable to permafrost thaw. *Proceedings of the National Academy of Sciences*, 117, 201916387. <https://doi.org/10.1073/pnas.1916387117>
- Hugelius, G., Strauss, J., Zubrzycki, S., Harden, J. W., Schuur, E. A. G., Ping, C.-L., et al. (2014). Estimated stocks of circumpolar permafrost carbon with quantified uncertainty ranges and identified data gaps. *Biogeosciences*, 11, 6573–6593. <https://doi.org/10.5194/bg-11-6573-2014>
- Hugelius, G., Virtanen, T., Kaverin, D., Pastukhov, A., Rivkin, F., Marchenko, S., et al. (2011). High-resolution mapping of ecosystem carbon storage and potential effects of permafrost thaw in periglacial terrain, European Russian Arctic. *Journal of Geophysical Research*, 116. <https://doi.org/10.1029/2010JG001606>
- Hyyppänen, H. (1996). Spatial autocorrelation and optimal spatial resolution of optical remote sensing data in boreal forest environment. *International Journal of Remote Sensing*, 17, 3441–3452. <https://doi.org/10.1080/01431169608949161>
- Ibañez, J. J., De-Albs, S., Bermúdez, F. F., & García-Álvarez, A. (1995). Pedodiversity: concepts and measures. *CATENA*, 24, 215–232. [https://doi.org/10.1016/0341-8162\(95\)00028-Q](https://doi.org/10.1016/0341-8162(95)00028-Q)
- Iversen, C. M., Sloan, V. L., Sullivan, P. F., Euskirchen, E. S., McGuire, A. D., Norby, R. J., et al. (2015). The unseen iceberg: plant roots in arctic tundra. *New Phytologist*, 205, 34–58. <https://doi.org/10.1111/nph.13003>
- Kimble, J. M., Tarnocai, C., Ping, C. L., Ahrens, R., Smith, C. A. S., Moore, J. P., & Lynn, W. (1993). Determination of the amount of carbon in highly cryoturbated soils. In D. Gilichinsky (Ed.), *Proceedings Joint Russian-American Seminar on Cryopedology and GlobalChange, Pushchino, Russia, 15–16 November 1992* (pp. 277–291). Moscow: Russian Academy of Sciences.
- Klaus, M., Becher, M., & Klaminder, J. (2013). Cryogenic soil activity along bioclimatic gradients in Northern Sweden: Insights from eight different proxies. *Permafrost and Periglacial Processes*, 24, 210–223. <https://doi.org/10.1002/ppp.1778>
- Köchy, M., Hiederer, R., & Freibauer, A. (2015). Global distribution of soil organic carbon—Part 1: Masses and frequency distributions of SOC stocks for the tropics, permafrost regions, wetlands, and the world. *SOIL*, 1, 351–365. <https://doi.org/10.5194/soil-1-351-2015>
- Kokelj, S. V., Smith, C. A. S., & Burn, C. R. (2002). Physical and chemical characteristics of the active layer and permafrost, Herschel Island, western Arctic Coast, Canada. *Permafrost and Periglacial Processes*, 13, 171–185. <https://doi.org/10.1002/ppp.417>
- Lantuit, H., & Pollard, W. H. (2005). Temporal stereophotogrammetric analysis of retrogressive thaw slumps on Herschel Island, Yukon Territory. *Natural Hazards and Earth System Sciences*, 5(3), 413–423. <http://dx.doi.org/10.5194/nhess-5-413-2005>
- Lantuit, H., & Pollard, W. H. (2008). Fifty years of coastal erosion and retrogressive thaw slump activity on Herschel Island, southern Beaufort Sea, Yukon Territory, Canada. *Geomorphology*, 95, 84–102.
- Lantuit, H., Pollard, W. H., Couture, N., Fritz, M., Schirmer, L., Meyer, H., & Hubberten, H.-W. (2012). Modern and late Holocene retrogressive thaw slump activity on the Yukon coastal plain and Herschel Island, Yukon Territory, Canada. *Permafrost and Periglacial Processes*, 23, 39–51.
- Lara, M. J., Nitze, I., Grosse, G., Martin, P., & McGuire, A. D. (2018). Reduced arctic tundra productivity linked with landform and climate change interactions. *Scientific Reports*, 8, 2345. <https://doi.org/10.1038/s41598-018-20692-8>
- Li, J., & Heap, A. D. (2014). Spatial interpolation methods applied in the environmental sciences: A review. *Environmental Modelling & Software*, 53, 173–189. <https://doi.org/10.1016/j.envsoft.2013.12.008>
- Li, J., Heap, A. D., Potter, A., & Daniell, J. J. (2011). Application of machine learning methods to spatial interpolation of environmental variables. *Environmental Modelling & Software*, 26, 1647–1659. <https://doi.org/10.1016/j.envsoft.2011.07.004>
- Liljedahl, A. K., Boike, J., Daanen, R. P., Fedorov, A. N., Frost, G. V., Grosse, G., et al. (2016). Pan-Arctic ice-wedge degradation in warming permafrost and its influence on tundra hydrology. *Nature Geoscience*, 9, 312–318. <https://doi.org/10.1038/ngeo2674>
- Lousada, M., Pina, P., Vieira, G., Bandeira, L., & Mora, C. (2018). Evaluation of the use of very high resolution aerial imagery for accurate ice-wedge polygon mapping (Adventdalen, Svalbard). *The Science of the Total Environment*, 615, 1574–1583. <https://doi.org/10.1016/j.scitotenv.2017.09.153>
- Mackay, J. R. (1959). Glacier ice-thrust features of the Yukon coast. *Geography Bulletin*, 13, 5–21.
- Matheron, G. (1963). Principles of geostatistics. *Economic Geology*, 58, 1246–1266.
- Matsuoka, N., Christiansen, H. H., & Watanabe, T. (2018). Ice-wedge polygon dynamics in Svalbard: Lessons from a decade of automated multi-sensor monitoring. *Permafrost and Periglacial Processes*, 29, 210–227. <https://doi.org/10.1002/ppp.1985>

- McBratney, A. B., Mendonça Santos, M. L., & Minasny, B. (2003). On digital soil mapping. *Geoderma*, *117*, 3–52. [https://doi.org/10.1016/S0016-7061\(03\)00223-4](https://doi.org/10.1016/S0016-7061(03)00223-4)
- Meerschman, E., Van Meirvenne, M., Van De Vijver, E., De Smedt, P., Islam, M. M., & Saey, T. (2013). Mapping complex soil patterns with multiple-point geostatistics. *European Journal of Soil Science*, *64*, 183–191. <https://doi.org/10.1111/ejss.12033>
- Michaelson, G. J., Ping, C. L., Epstein, H., Kimble, J. M., & Walker, D. A. (2008). Soils and frost boil ecosystems across the North American Arctic Transect. *Journal of Geophysical Research*, *113*, G03S11.
- Minasny, B., McBratney, A. B., & Hartemink, A. E. (2010). Global pedodiversity, taxonomic distance, and the World Reference Base. *Geoderma*, *155*, 132–139. <https://doi.org/10.1016/j.geoderma.2009.04.024>
- Mishra, U., Jastrow, J. D., Matamala, R., Hugelius, G., Koven, C. D., Harden, J. W., et al. (2013). Empirical estimates to reduce modeling uncertainties of soil organic carbon in permafrost regions: a review of recent progress and remaining challenges. *Environmental Research Letters*, *8*, 035020. <https://doi.org/10.1088/1748-9326/8/3/035020>
- Mishra, U., & Riley, W. J. (2015). Scaling impacts on environmental controls and spatial heterogeneity of soil organic carbon stocks. *Biogeosciences*, *12*, 3993–4004. <https://doi.org/10.5194/bg-12-3993-2015>
- Myers-Smith, I. H., Forbes, B. C., Wilmking, M., Hallinger, M., Lantz, T., Blok, D., et al. (2011). Shrub expansion in tundra ecosystems: dynamics, impacts and research priorities. *Environmental Research Letters*, *6*, 045509. <https://doi.org/10.1088/1748-9326/6/4/045509>
- Myneni, R. B., Keeling, C. D., Tucker, C. J., Asrar, G., & Nemani, R. R. (1997). Increased plant growth in the northern high latitudes from 1981 to 1991. *Nature*, *386*, 698–702. <https://doi.org/10.1038/386698a0>
- Obu, J., Lantuit, H., Myers-Smith, I., Heim, B., Wolter, J., & Fritz, M. (2015). Effect of Terrain Characteristics on Soil Organic Carbon and Total Nitrogen Stocks in Soils of Herschel Island, Western Canadian Arctic. *Permafrost and Periglacial Processes*, *16*. <https://doi.org/10.1002/ppp.1881>
- Oliver, M. A., & Webster, R. (2015). *Basic steps in geostatistics: The variogram and Kriging*, SpringerBriefs in Agriculture. Cham: Springer International Publishing. <https://doi.org/10.1007/978-3-319-15865-5>
- Olofsson, J., & Post, E. (2018). Effects of large herbivores on tundra vegetation in a changing climate, and implications for rewilding. *Philosophical Transactions of the Royal Society B: Biological Sciences*, *373*, 20170437. <https://doi.org/10.1098/rstb.2017.0437>
- Palmtag, J., & Kuhry, P. (2018). Grain size controls on cryoturbation and soil organic carbon density in permafrost-affected soils. *Permafrost and Periglacial Processes*, *29*, 112–120.
- Pastick, N. J., Rigge, M., Wylie, B. K., Jorgenson, M. T., Rose, J. R., Johnson, K. D., & Ji, L. (2014). Distribution and landscape controls of organic layer thickness and carbon within the Alaskan Yukon River Basin. *Geoderma*, *230*, 79–94.
- Phillips, J. D. (1988). The role of spatial scale in geomorphic systems. *Geographical Analysis*, *20*, 308–317. <https://doi.org/10.1111/j.1538-4632.1988.tb00185.x>
- Ping, C.-L., Clark, M. H., Kimble, J. M., Michaelson, G. J., Shur, Y., & Stiles, C. A. (2013). Sampling Protocols for Permafrost-Affected Soils. *Soil Horizons*, *54*, 13. <https://doi.org/10.2136/sh12-09-0027>
- Ping, C. L., Jastrow, J. D., Jorgenson, M. T., Michaelson, G. J., & Shur, Y. L. (2015). Permafrost soils and carbon cycling. *SOIL*, *1*, 147–171. <https://doi.org/10.5194/soil-1-147-2015>
- Ping, C. L., Michaelson, G. J., Jorgenson, M. T., Kimble, J. M., Epstein, H., Romanovsky, V. E., & Walker, D. A. (2008). High stocks of soil organic carbon in the North American Arctic region. *Nature Geoscience*, *1*, 615–619. <https://doi.org/10.1038/ngeo284>
- Ping, C. L., Michaelson, G. J., & Kimble, J. M. (1997). Carbon storage along a latitudinal transect in Alaska. *Nutrient Cycling in Agroecosystems*, *49*, 235–242.
- Ping, C. L., Michaelson, G. J., Kimble, J. M., Romanovsky, V. E., Shur, Y. L., Swanson, D. K., & Walker, D. A. (2008). Cryogenesis and soil formation along a bioclimate gradient in Arctic North America. *Journal of Geophysical Research: Biogeosciences*, *113*, 2005–2012. <https://doi.org/10.1029/2008JG000744>
- Pope, A., Rees, W. G., Fox, A. J., & Fleming, A. (2014). Open access data in polar and cryospheric. *Remote Sensing*, *6*, 6183–6220. <https://doi.org/10.3390/rs6076183>
- R Core Team. (2020). *R: A language and environment for statistical computing*. Vienna, Austria: R Foundation for Statistical Computing.
- Ramage, J. L., Fortier, D., Hugelius, G., Lantuit, H., & Morgenstern, A. (2019). Distribution of carbon and nitrogen along hillslopes in three valleys on Herschel Island, Yukon Territory, Canada. *CATENA*, *178*, 132–140.
- Sarma, D. D. (2009). *Geostatistics with applications in earth sciences* (2nd ed.). Dordrecht: Springer.
- Schoeneberger, P. J., Wysocki, D. A., Benham, E. C., & Soil Survey Staff. (2012). *Field book for describing and sampling soils, version 3.0*. Natural resources conservation service. Lincoln, NE: National Soil Survey Center.
- Schuur, E. A. G., McGuire, A. D., Schädel, C., Grosse, G., Harden, J. W., Hayes, D. J., et al. (2015). Climate change and the permafrost carbon feedback. *Nature*, *520*, 171–179. <https://doi.org/10.1038/nature14338>
- Siewert, M. B. (2018). High-resolution digital mapping of soil organic carbon in permafrost terrain using machine learning: a case study in a sub-Arctic peatland environment. *Biogeosciences*, *15*, 1663–1682. <https://doi.org/10.5194/bg-15-1663-2018>
- Siewert, M. B., Hanisch, J., Weiss, N., Kuhry, P., Maximov, T. C., & Hugelius, G. (2015). Comparing carbon storage of Siberian tundra and taiga permafrost ecosystems at very high spatial resolution: Ecosystem carbon in taiga and tundra. *Journal of Geophysical Research: Biogeosciences*, *120*, 1973–1994. <https://doi.org/10.1002/2015JG002999>
- Siewert, M. B., Hugelius, G., Heim, B., & Faucherre, S. (2016). Landscape controls and vertical variability of soil organic carbon storage in permafrost-affected soils of the Lena River Delta. *CATENA*, *147*, 725–741. <https://doi.org/10.1016/j.catena.2016.07.048>
- Siewert, M. B., & Olofsson, J. (2020). Scale-dependency of Arctic ecosystem properties revealed by UAV. *Environmental Research Letters*. <https://doi.org/10.1088/1748-9326/aba20b>
- Sjöberg, Y., Siewert, M. B., Rudy, A. C. A., Paquette, M., Bouchard, F., Malenfant-Lepage, J., & Fritz, M. (2020). Hot trends and impact in permafrost science. *Permafrost and Periglacial Processes*. <https://doi.org/10.1002/ppp.2047>
- Smith, C. S., Kennedy, C. E., Hargrave, A. E., & McKenna, K. M. (1989). *Soil and vegetation of Herschel island, Yukon territory, Yukon soil survey report No. 1 LRRC contribution No. 88-26*. Yukon: Agriculture Canada, Whitehorse.
- Soil Classification Working Group. (1998). *The Canadian system of soil classification*. Ottawa, ON: Agriculture and Agri-Food Canada PublicationNRC Research Press, National Research Council of Canada.
- Soil Survey Staff. (2014). *Keys to soil taxonomy* (12th ed.). Washington, DC: United States Department of Agriculture & Natural Resources Conservation Service.
- Tarnocai, C., Canadell, J. G., Schuur, E. A. G., Kuhry, P., Mazhitova, G., & Zimov, S. (2009). Soil organic carbon pools in the northern circumpolar permafrost region. *Global Biogeochemical Cycles*, *23*, 11. <https://doi.org/10.1029/2008GB003327>
- Taş, N., Prestat, E., Wang, S., Wu, Y., Ulrich, C., Kneafsey, T., et al. (2018). Landscape topography structures the soil microbiome in arctic polygonal tundra. *Nature Communications*, *9*, 777. <https://doi.org/10.1038/s41467-018-03089-z>

- Tobler, W. R. (1970). A computer movie simulating urban growth in the detroit region. *Economic Geography*, *46*, 234–240. <https://doi.org/10.2307/143141>
- Tumel, Z. (2019). Diagnostics and mapping of geocological situations in the permafrost zone of Russia. *Geosciences*, *9*, 353. <https://doi.org/10.3390/geosciences9080353>
- Turetsky, M. R., Abbott, B. W., Jones, M. C., Anthony, K. W., Olefeldt, D., Schuur, E. A. G., et al. (2020). Carbon release through abrupt permafrost thaw. *Nature Geoscience*, *13*, 138–143. <https://doi.org/10.1038/s41561-019-0526-0>
- Ulrich, M., Grosse, G., Strauss, J., & Schirrmeyer, L. (2014). Quantifying wedge-ice volumes in Yedoma and Thermokarst Basin Deposits. *Permafrost and Periglacial Processes*, *25*, 151–161. <https://doi.org/10.1002/ppp.1810>
- Ulrich, M., Hauber, E., Herzschuh, U., Härtel, S., & Schirrmeyer, L. (2011). Polygon pattern geomorphometry on Svalbard (Norway) and western Utopia Planitia (Mars) using high-resolution stereo remote-sensing data. *Geomorphology*, *134*, 197–216. <https://doi.org/10.1016/j.geomorph.2011.07.002>
- Walker, D. A., Epstein, H. E., Gould, W. A., Kelley, A. M., Kade, A. N., Knudson, J. A., et al. (2004). Frost-boil ecosystems: complex interactions between landforms, soils, vegetation and climate. *Permafrost and Periglacial Processes*, *15*, 171–188. <https://doi.org/10.1002/ppp.487>
- Walker, D. A., Epstein, H. E., Romanovsky, V. E., Ping, C. L., Michaelson, G. J., Daanen, R. P., et al. (2008). Arctic patterned-ground ecosystems: A synthesis of field studies and models along a North American Arctic Transect. *Journal of Geophysical Research*, *113*. <https://doi.org/10.1029/2007JG000504>
- Warburton, J. (2013). 8.19 Patterned ground and polygons. In *Treatise on geomorphology* (pp. 298–312). Elsevier.
- Washburn, A. L. (1956). Classification of patterned ground and review of suggested origins. *The Geological Society of America Bulletin*, *67*, 823–866. [https://doi.org/10.1130/0016-7606\(1956\)67\[823:COPGAR\]2.0.CO;2](https://doi.org/10.1130/0016-7606(1956)67[823:COPGAR]2.0.CO;2)
- Webster, R., & Oliver, M. A. (1992). Sample adequately to estimate variograms of soil properties. *Journal of Soil Science*, *43*, 177–192. <https://doi.org/10.1111/j.1365-2389.1992.tb00128.x>
- Webster, R., & Oliver, M. A. (2007). *Geostatistics for environmental scientists* (2nd ed.). Cornwall: John Wiley & Sons.
- Weindorf, D. C., & Zhu, Y. (2010). Spatial variability of soil properties at Capulin Volcano, New Mexico, USA: Implications for sampling strategy. *Pedosphere*, *20*, 185–197. [https://doi.org/10.1016/S1002-0160\(10\)60006-9](https://doi.org/10.1016/S1002-0160(10)60006-9)
- Weiss, N., Blok, D., Elberling, B., Hugelius, G., Jørgensen, C. J., Siewert, M. B., & Kuhry, P. (2016). Thermokarst dynamics and soil organic matter characteristics controlling initial carbon release from permafrost soils in the Siberian Yedoma region. *Sedimentary Geology*, *340*, 38–48. <https://doi.org/10.1016/j.sedgeo.2015.12.004>
- Wolter, J., Lantuit, H., Fritz, M., Macias-Fauria, M., Myers-Smith, I., & Herzschuh, U. (2016). Vegetation composition and shrub extent on the Yukon coast, Canada, are strongly linked to ice-wedge polygon degradation. *Polar Research*, *35*, 27489. <https://doi.org/10.3402/polar.v35.27489>
- Zhang, W., Weindorf, D. C., & Zhu, Y. (2011). Soil organic carbon variability in croplands: Implications for sampling design. *Soil Science*, *176*, 367. <https://doi.org/10.1097/SS.0b013e31821eb7d2>
- Zoltai, S. C., & Tarnocai, C. (1981). Some nonsorted patterned ground types in Northern Canada. *Arctic and Alpine Research*, *13*, 139. <https://doi.org/10.2307/1551191>